Title

Mechanical Properties and Chemical Reactivity of Li x SiO y Thin Films

Journal
ACS Applied Materials & Interfaces, 10(44)

ISSN
1944-8244

Authors
Xu, Yun
Stetson, Caleb
Wood, Kevin
et al.

Publication Date
2018-11-07

DOI
10.1021/acsami.8b10895

Peer reviewed

Mechanical Properties and Chemical Reactivity of Li_xSiO_y Thin Films

*Yun Xu [a], Caleb Stetson [b,c], Kevin Wood [a], Eric Sivonxay [d] , Chunsheng Jiang [a], Glenn Teeter [a], Svitlana Pylypenko [c], Sang-Don Han [b], Kristin A. Persson [d,e], Anthony Burrell [b], Andriy Zakutayev [a]**

[a] Materials Science Center, National Renewable Energy Laboratory, Golden, CO, 80401, USA

[b] Chemistry and Nanoscience Center, National Renewable Energy Laboratory, Golden, CO, 80401, USA

[c] Department of Chemistry, Colorado School of Mines, Golden, CO, 80401, USA

[d] Lawrence Berkeley National Laboratory, Berkeley, CA 94720, USA

[e] Department of Materials Science & Engineering, University of California, Berkeley, CA 94720-1760, USA

KEYWORDS: mechanical properties, chemical reactivity, solid electrolyte interphases, Li_xSiO_y, lithium ion batteries

ABSTRACT: Silicon (Si) is a commonly studied candidate material for next-generation anodes in Li-ion batteries. A native oxide SiO_2 on Si is often inevitable. However, it is not clear if this layer has positive or negative effect on the battery performance. This understanding is complicated by the lack of knowledge about the physical properties of the SiO_2 lithiation products, and by convolution of chemical and electrochemical effects during the anode lithiation process. In this study, Li_xSiO_y thin films as model materials for lithiated SiO_2 were deposited by magnetron sputtering at ambient temperature, with the goal of 1) decoupling chemical reactivity from electrochemical reactivity, and 2) evaluating the physical and electrochemical properties of Li_xSiO_y. XPS analysis of the deposited thin films demonstrate that a composition close to previous experimental reports of lithiated native SiO_2, can be achieved through sputtering. Our density functional theory calculations also confirm that possible phases formed by lithiating SiO_2 are very close to the measured film compositions. Scanning probe microscopy measurements show the mechanical properties of the film are strongly dependent on lithium concentration, with ductile behavior and higher Li content, and brittle behavior at lower Li content. Chemical reactivity of the thin films was investigated by measuring AC impedance evolution, suggesting that Li_xSiO_y continuously reacts with electrolyte, in part due to high electronic conductivity of the film determined from solid state impedance measurements. Electrochemical cycling data of sputter deposited Li_xSiO_y/Si films also suggest that Li_xSiO_y is not beneficial in stabilizing the Si anode surface during battery operation, despite its favorable mechanical properties.

Introduction

Silicon (Si) is considered to be one of the leading candidates for the next generation anode materials in Li-ion batteries, as it features a theoretical capacity more than 10 times higher than graphite.[1] However, one of the major challenges of silicon is the large volume change during the lithiation and delithiation processes. This volume change eventually leads to the breakdown of the solid electrolyte interphase (SEI), and further reactions that cause increased electrolyte consumption, higher interphase resistance, and the ultimate failure of the cell.[2]

There have been extensive studies on the SEI formation on the surface of silicon.[3] While various reports on the overall composition of the SEI are reaching some consensus, the understanding of its physical properties and chemical reactivity is still limited. Most work is focused on the SEI composition through characterization by Fourier Transform Infrared Reflectance (FTIR), and X-ray Photoemission Spectroscopy (XPS),[4-9] while less research has been done to separately study SEI properties independent of the electrode[10]. Theoretically, a good SEI should be flexible or soft enough to accommodate the large volumetric change of the silicon. In addition to the mechanical properties of the SEI, high ionic conductivity and low electronic conductivity are also important factors in determining if a certain phase is beneficial to electrode stability.

It has been hypothesized, that one of the most important SEI components for Si anodes in Li-ion batteries is Li_xSiO_y, which originates from the lithiation of the native oxide on Si (SiO_2). The role of SiO_2 on a Si anode is controversial: on one hand, it confines the volume expansion of Si, while on the other hand it induces interfacial reactions that

consume lithium in the electrolyte. Lithiation of SiO_2 is a complicated process, and the products depend on the charge state of the battery. [11-13] General findings are SiO_2 can be reduced to possible products of $Li_2Si_2O_5$, Li_4SiO_4, Li_2O, Si, and Li_xSi.[10] Nevertheless, most of the recent model system studies are focused on the fully oxidized lithium silicates such as Li_4SiO_4, Li_2SiO_3, $Li_2Si_2O_5$.[7, 14-16]

In this work, the mechanical and electrochemical properties, as well as the chemical reactivity of the composite Li_xSiO_y film are investigated. For this purpose, a special combinatorial Li_xSiO_y composite film with composition close to the lithiated SiO_2 was synthesized by reactive sputtering, allowing to study its mechanical properties without any effect from electrolyte decomposition products. According to XPS results, both the lithium-rich and silicon-rich areas consist of lithium silicates, some Li_xSi_y and very little SiO_2. The film compositions agree well with the phase diagram predicted by DFT calculations. It is found that the composite Li_xSiO_y film exhibits relatively-high electronic conductivity and low hardness, based on scanning probe microscopy results and impedance measurements. Computed bulk moduli shows the same trend as the experimental results, specifically that higher Li content leads to lower moduli. To evaluate the chemical reactivity of these materials, a multilayer thin film Li_xSiO_y on Si was measured using impedance spectroscopy in a coin cell followed by electrochemical charge/discharge cycling. The results indicate that the composite film is unable to fully passivate the Si surface, due to its high electronic conductivity, and despite its ductile mechanical properties.

Methods

Li_xSiO_y thin films were synthesized by RF magnetron sputtering (13.56MHz) using lithium target (Lesker, 99.9%, 2" diameter) and silicon target (Lesker, 99.999%, 3" diameter). The lithium target was cleaned with hexane (99.9%) before use to remove residual mineral oil, which protects lithium target from being oxidized during the shipment. Furthermore, oxidized film on top of lithium target was periodically removed by Dremel tool with copper brush. During the deposition, 30 W RF power was applied to both lithium and silicon targets. Copper foil and Eagle XG glass were used as substrate for electrochemical measurement and scanning probe microscopy measurement respectively. To generate plasma, Ar (99.999% purity) was introduced at a constant pressure of 3 mTorr into a vacuum chamber with $3x10^{-8}$ Torr base pressure. The film was deposited at room temperature, so it is expected to be amorphous (also confirmed by x-ray diffraction). After the synthesis, the samples were removed from a chamber to a glovebox. Airless transfer in a vacuum vessel to all characterization instruments was adopted because of the high reactivity of Li_xSiO_y. As a reference for comparison, thin films of Li-free Si and Li_xSiO_y/Si were made using the same method.

The XPS measurements were performed using a glovebox-integrated Phi 5600 XPS system. Glovebox conditions were better than <10 ppm moisture and O_2. Base pressures for the Phi 5600 XPS system was below 7×10^{-10} Torr. Photoelectrons were generated using monochromatic Al Kα X-ray excitation (1486.7 eV). The spectrometer binding-energy (BE) scale was calibrated by measuring valence-band and core-level spectra from sputter-cleaned Au, Ag, and Cu foils (EF = 0.00 eV, Au 4f7/2 = 83.96 eV, Ag 3d5/2 = 368.26 eV,

and Cu 2p3/2 = 932.62 eV).[17] Ar^+ sputtering (incident energy 3keV) was used for depth profiling. Curve fitting and data processing were performed using Igor Pro with a custom program adapted from literature.[18]

Scanning probe microscopy (SPM) techniques have been used to evaluate mechanical and electrical properties of the thin films. Nanoindentation experiments were performed in an argon-filled glovebox with an atomic force microscope (AFM, Veeco D5000 and Nanoscope V) using Bruker DDESP diamond-coated Si probe in contact mode. Changing deflection set-points applied to the tip allows the force to be controlled based on deflection versus z-distance calibration curves. For these experiments, four sites with different lithium concentration were indented with varied indentation forces. Each indentation duration was held for 10 seconds. After unloading the indentation, tapping mode AFM surface morphology images were taken and the indentation depths were measured.

Electrochemical properties were investigated by making coin cells and performing impedance spectroscopy measurement and galvanostatic cycling. The thin film samples with 14mm diameter were punched out from the silicon-rich region and lithium-rich region. The electrolyte was 1.2M $LiPF_6$ in a 1:1 (volume) ethylene carbonate (EC) and dimethyl carbonate (DMC) mixture. Lithium metal was used as counter/reference electrode. The cells were first charged to 1.5V (vs. Li^+ /Li hereafter) and then discharged to 50mV. Impedance evolution was investigated by collecting spectrums of a fresh electrode and an exposed electrode to an electrolyte for 24 hours, respectively. AC impedance data of a coin cell was collected in a frequency range of 100KHz to 10mHz.

The solid-state AC impedance data of thin films deposited on interdigitated platinum electrodes were collected in a frequency range of 1MHz to 1Hz.

Phase stability was examined computationally by constructing a phase diagram from density functional theory (DFT) calculations. DFT calculations were performed, using the Vienna Ab-initio Simulation Package (VASP)[19-20], on known crystalline phases in the Li-Si-O system, found on the Materials Project.[19] Calculations used the Projector Augmented Wave (PAW) method with the Generalized Gradient Approximation(GGA) Perdew-Burke-Ernzerhof (PBE) framework.[21-22] Structure optimization calculations allowed all atomic positions and lattice parameters to relax. DFT calculations parameters plane wave cutoff of 520 eV and a minimum reciprocal lattice k-point density of 64 / $Å^3$. The Python Materials Genomics package (pymatgen) was used to construct phase diagram of the Li_xSiO_y system.[23-24] Additionally, bulk moduli were computed by fitting the Rose-Vinet equation[25] of state to the calculated energies and volumes of a series of deformed structures for the amorphous materials.

Results and Discussion

Deposition and characterization

High-throughput experimental combinatorial methods have been applied in materials science for discovery and optimization of various functional materials[26-27]. These methods are also well suited to electrochemical applications such as fuel cells and lithium ion batteries.[28-29] In this work, a combinatorial approach was applied to screen properties of lithium silicon compounds with different composition. The combinatorial

chamber geometry is depicted in Figure 1. The lithium target was 8 cm away facing the substrate, and silicon target was 12 cm at an angle with respect to the substrate. Due to this geometry, the deposited films have higher Si/Li ratio in the region closer to silicon source, and lower Si/Li ratio in the region further from the silicon source. From these experiments, we found that the target to substrate distance has strong effect on the oxygen content in the film: the shorter the target-substrate distance is, the lower the oxygen content is. This trend can be explained by the decreased reaction of lithium plasma particles with oxygen contaminants in the chamber resulting from H_2O base pressure. Further, the oxygen content in the film can be minimized by increasing the deposition rate by increasing the power applied to Li and Si targets. However, the power applied to Li target cannot be too high to avoid Li melting.

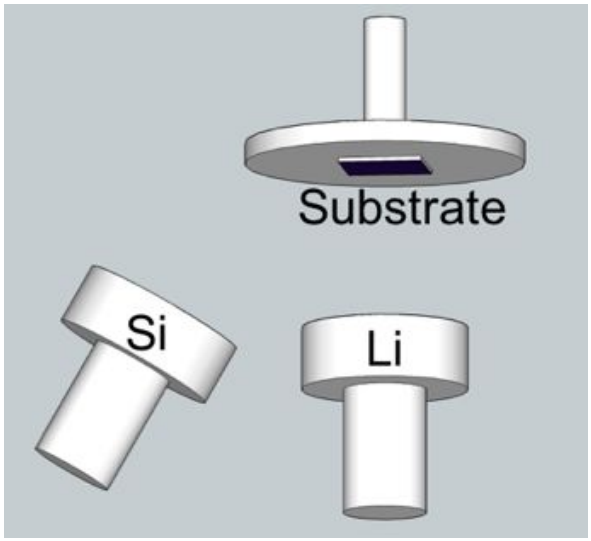

Figure 1. Chamber geometry used to deposit Li_xSiO_y thin films

In Figure 2, depth profiles are shown for Li1s, Si2p and O1s core level spectra, for both lithium-rich and silicon-rich regions of the thin film. From the XPS depth-profile,

significant oxidation was observed at the surface, even though the samples were protected from ambient atmosphere during the transfer from the deposition to the characterization instrument. Figure S1 shows the experimental spectra (and the corresponding peak fits) obtained from the bulk of the film. Compositions obtained via peak-fitting these spectra are listed in Table S1. As can be seen from the XPS fitting results in Table S1, for both lithium-rich and silicon-rich side of the film, lithium silicate and lithium silicide are the main components in the film, with some contribution from SiO_2. The average compositions for lithium-rich area and silicon-rich area are $Li_{4.88}Si_{2.85}O_{2.52}$ and $Li_{1.58}Si_{1.31}O_{1.95}$, respectively. Hence, the thin film is subsequently referred to as a Li_xSiO_y composite film. We note that the lithium-rich area has more lithium and more O compared to the silicon-rich area. Higher oxygen content in lithium-rich area results from the higher affinity of lithium to oxygen.

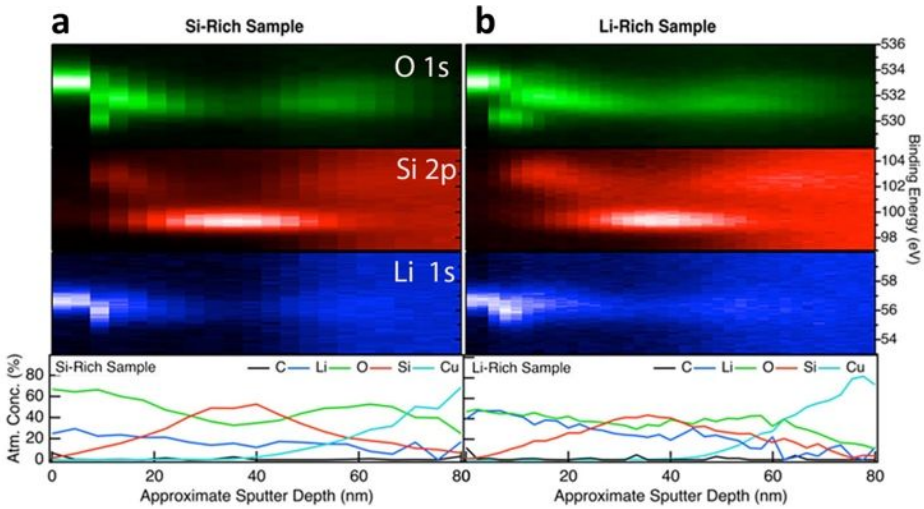

Figure 2. XPS depth profile analysis of Li_xSiO_y composite thin film on copper foil for (a) Si-rich region, and (b) Li-rich region. The top panels show binding energy depth profile

of O 1s (green); Si 2p (red); Li 1s (blue). The bottom panel shows atomic percentage as a function a sputter depth.

The ternary phase diagram in Figure 3 shows the stability of crystalline compositions within the Li-Si-O phase space as predicted by DFT calculations. Nodes represent compositions of stable crystalline phases, while lines and triangles depict two-phase and 3 phase regions, respectively. The "phase diagram" of the amorphous structures is much more difficult to calculate, but it may be expected to be similar. Following the dashed line, the phase diagram predicts the possible lithiation products of SiO_2 to be lithium silicides, lithium silicates and Li_2O depending on the degree of lithiation. For example, fully lithiated SiO_2 is predicted as a mixture of $Li_{21}Si_5$, Li, and Li_2O. The films studied in this work are amorphous according to x-ray diffraction, and thus can be considered as the lithiation products of the amorphous SiO_2 layer on Si surface. Observed lithium-rich and silicon-rich areas represent different lithiation stages of the SiO_2 film.

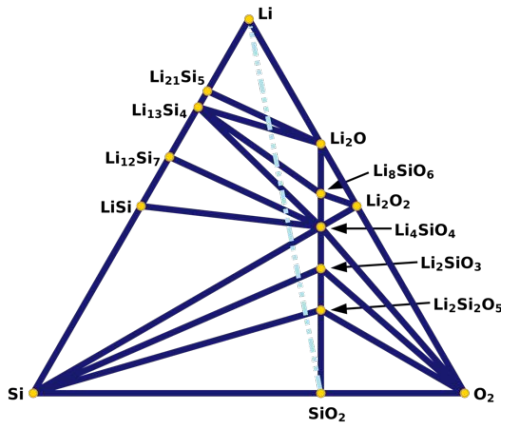

Figure 3. Phase diagram of Li-Si-O_2 system at 0K. The dashed blue line indicates predicted lithiation trajectory from SiO_2.

Scanning probe microscopy (SPM)

SPM-based nano-indentation measurements were performed on Li_xSiO_y thin films and a reference Si sample. Surface morphology is depicted in Figure S2a, indicating film roughness of 20 nm in an area 0.5 μm by 0.5 μm. Figure S2b shows typical residual indentation imprints of film reflecting the film behavior upon different force loads.

The mechanical response from the lithium-rich and silicon-rich Li_xSiO_y are shown in Figure 4a. In the lithium-rich area, a linear increase of indentation depth with the load was observed in a force range of 5-55 μN, indicating ductile behaviour. In contrast, the silicon-rich area of Li_xSiO_y shows a brittle behaviour: here the probe easily broke through the film and the cracks propagated, independent on the load in the force range. Figure 4b shows a scan in AFM height mode of the six indentation points on both silicon-rich and lithium-rich regions. The magnified images in both height and phase AFM modes (Figure S3) also show difference between ductile and brittle behavior.

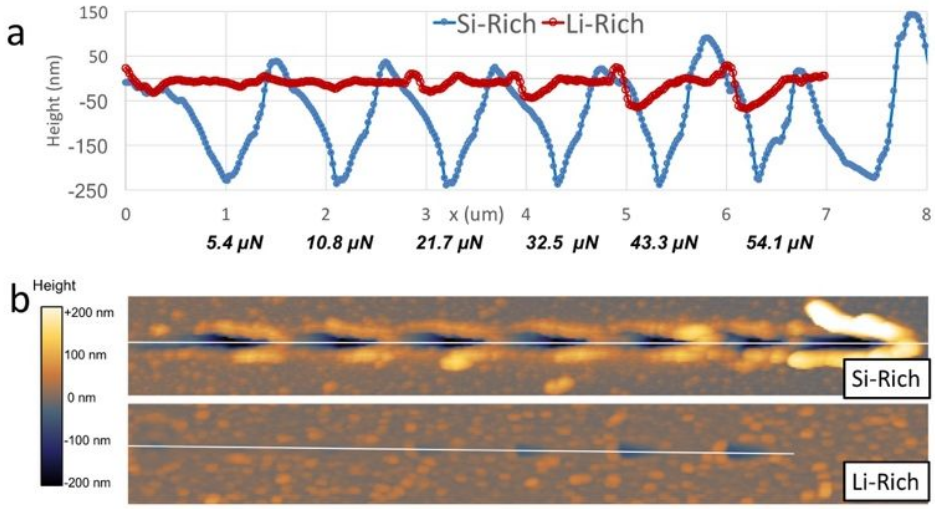

Figure 4. a) Indentation depth at different sites with increasing indentation force aligned with each valley in the curve; b) AFM images of indented film at both silicon-rich and lithium-rich regions.

To visualize the transition better, the indentation depth is plotted against the changing lithium concentration in the combinatorial sample in Figure S4. An inflection point, where the indentation depth increases sharply at low Li content, is due to cracking of the film in a brittle manner. Computational results for the different amorphous structure configurations (see Figure 5) confirms this trend: higher lithium concentration both in Si and SiO_2 causes a decrease of the bulk moduli. We note that the film is composed of both lithium silicide and lithium silicates and hence it combines the mechanical properties of both materials. Incidentally, the film composition falls close to the critical transition point of Li/Si=1:1. Reference crystalline Si showed a very hard behavior, i.e., the indentation depth is 0 nm.

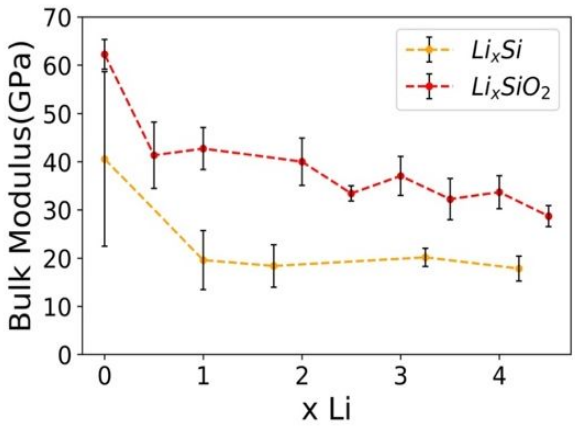

Figure 5. Calculated bulk moduli of lithiated silicon and lithiated SiO_2 plotted against the degree of lithiation of these amorphous structures. Error bars correspond to the different configurations of the amorphous structure.

Electrochemical impedance and cycling

To obtain further insight into the chemical reactivity of Li_xSiO_y composite films, a 50nm thick sample was assembled into a coin cell and investigated by impedance spectroscopy and by galvanostatic charge and discharge measurements (Figure 6). Capacity is not normalized in this work since all the films have the same thickness and area. As shown in Figure 6a, a low amount of lithium could be extracted from the film even up to 1.5V during the first charge cycle. This high OCV is due to the lower electrochemical potential of lithium in Li_xSiO_y which has part of lithium bonded with oxygen. To investigate the reaction of the Li_xSiO_y composite film with electrolyte, it was measured by AC impedance at the open circuit voltage, as shown in Figure 6b. When the Li_xSiO_y composite film comes into contact with electrolyte, the charge transfer resistance

increases with time. In contrast, for the silicon electrode the impedance is not time dependent at open circuit voltage.

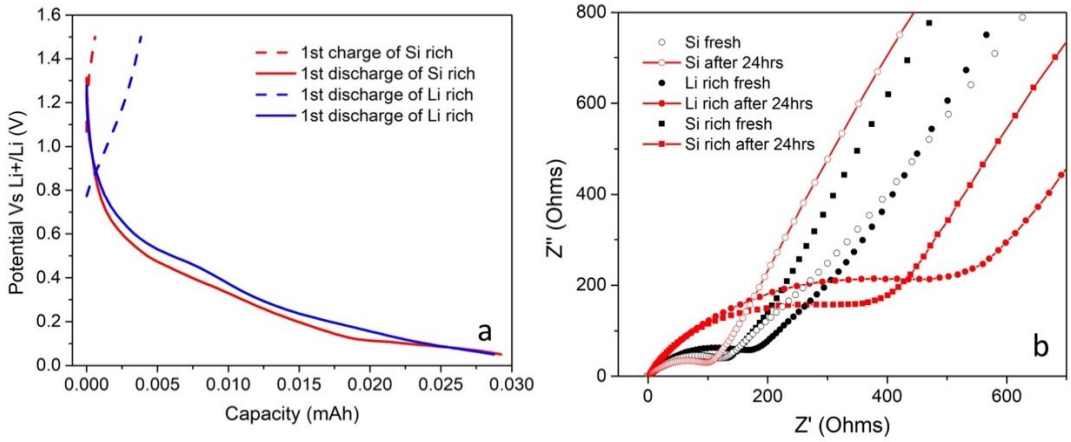

Figure 6. a) Voltage profile of lithium-rich Li_xSiO_y composite film and silicon-rich Li_xSiO_y composite film; b) Impedance evolution of lithium-rich Li_xSiO_y composite and silicon-rich Li_xSiO_y composite as well as Si film.

The higher charge transfer resistance of Li_xSiO_y, as compared to Si, is likely to originate from the resulting Li_xSiO_y surface-electrolyte interface. The higher the lithium concentration in the compound, the lower the potential vs. lithium, which promotes reduction reactions with the electrolyte. During charging, as SiO_2 is lithiated to LixSiOy, this increased reactivity may lead to further consumption of electrolyte if Li_xSiO_y is exposed and not fully covered with the other chemically stable electrolyte decomposition products. There has been literature [30] discussing reduction mechanisms of ethylene carbonate on the lithium silicide surface which identify different mechanisms depending on the degree of lithiation. Higher concentration of lithium was found to be more reactive due to the explicit interaction of EC molecules with Li^+ ions at the surface. In addition,

recent experiment work by our group found that both lithium silicide and lithium silicate react with electrolyte, and form fluoride and carbonate species which are commonly seen in the SEI components.[31-32] Computational work also demonstrate that chemistry-dependent interaction happens on the surface of lithium silicide with electrolyte.[33] We note that increased lithiation of SiO_2 leads to increased reactivity with the electrolyte, and consumes lithium inventory.

Impedance of the as-prepared Li_xSiO_y thin film on interdigitated electrode (without any electrolyte exposure) is shown in Figure S5. This thin film behaves like a pure resistor, which is mainly due to the existence of lithium silicide in the film. Total conductivity is dominated by electronic conductivity. The total conductivity of a LixSiOy thin film is calculated as

$$\sigma = L/(R*A)$$

where σ is the conductivity, L is the distance between the Pt digits and A is the total contacting area. The conductivity σ is calculated to be 2.7 S/cm, which is too high to be a good SEI layer.

To correlate the measured Li_xSiO_y properties with the electrochemical cycling performance of an electrode with Li_xSiO_y at the surface, a double layer sample was deposited with Li_xSiO_y on top of a silicon thin film, and compared to a Si film. The thickness of Li_xSiO_y was set to 10 nm to emulate the native oxide thickness, and the thickness of silicon thin film was set to 50 nm, as shown in the inset in Figure 7a. As shown in Figure 7a, during the first cycle discharge profile, Li_xSiO_y /Si exhibited a lower OCV of only 1.5 V (comparted to 2.5 V for Si), due to the existing lithium on the silicon

surface. The difference of the CV profiles above 0.25V (before Si starts lithiating) results from the surface reaction between Li_xSiO_y and electrolyte. Both low potential of Li_xSiO_y and its reaction products make the electrochemical reduction different than that in the silicon case. The lower potential range profiles for both films are very similar, since the same thickness of silicon film was deposited. The cycling of Li_xSiO_y/Si showed a lower columbic efficiency and less stable performance as compared to the bare silicon (see Figure 7b). We note that the columbic efficiency of silicon is higher than that of the Li_xSiO_y -coated Si, indicating that the Li_xSiO_y film exhibits a greater reactivity with electrolyte. We hypothesize that the Li_xSiO_y composite film continuously reacts with the electrolyte, preventing the stabilization of the SEI on the silicon electrode. These results suggest that SiO_2 does not help stabilize the surface of the Si electrode, as the lithiation products are not stable upon cycling. Previously, there has been study[34] the effect of SiO_2 with various thickness from 2nm, 7nm to 10nm. Only the 7nm SiO_2 coated Si showed the improved performance compared to Si. This is a complimentary result from both mechanical property and reactivity. More studies of the reactant product between Li_xSiO_y and electrolyte are in progress to clarify the role of Li_xSiO_y in the functionality and SEI stabilization of the Si anode.

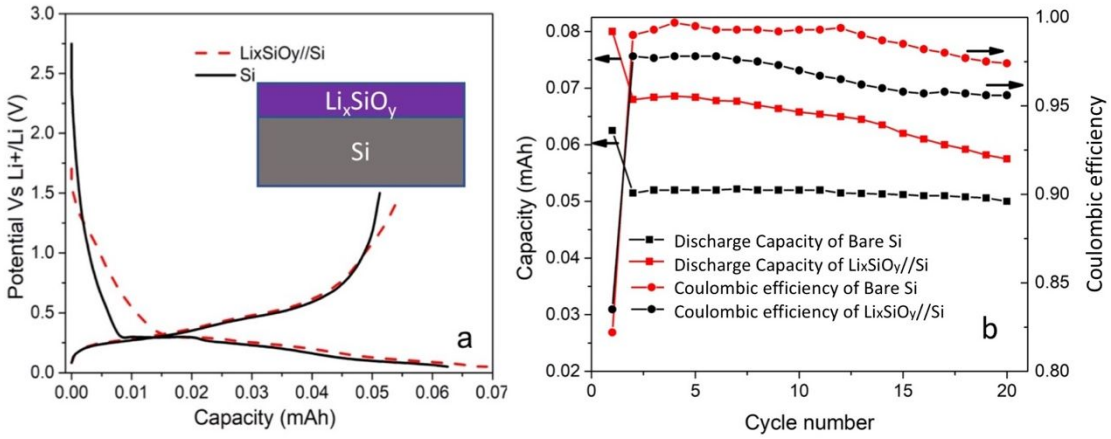

Figure 7. a) Charge and discharge profile of Si and Li_xSiO_y /Si, with inset picture shows the schematic of double layer thin film; b) Cycle performance and Columbic efficiency of double layer thin film and pure silicon.

Conclusions

In summary, mechanical and electrochemical properties, as well as the chemical reactivity of the Li_xSiO_y composite thin film with Li to Si ratio between 1.7 and 1.1 were investigated. These Li_xSiO_y films with Li-rich and Si-rich compositions were prepared by combinatorial sputtering, as a model system to study the initial products of lithiation of native oxide SiO_2 layer on a Si anode, relevant for next-generation Li-ion batteries. First-principles computational results show that both lithiated silicon and lithiated SiO_2 transition from brittle to ductile behavior as lithiation happens. The as-synthesized composite Li_xSiO_y film, which is a mixture of lithium silicides and lithium silicates, shows an equivalent brittle to ductile transition. The intermediate product of lithiated SiO_2, which contains lithium silicates and lithium silicates, is highly reactive with the electrolyte, due to the low potential resulting from high lithium content. These composite

Li_xSiO_y with Li/Si=1.7 and Li/Si=1.1 showed low electronic resistance and did not facilitate the passivation and stabilization of the Si films, despite their low resistance to fracture. Thus, a favorable ductile mechanical property is found to be a desirable but insufficient criterion for stable SEI formation; low chemical reactivity and low electronic conductivity are also important for stable electrodes.

ASSOCIATED CONTENT

Supporting Information. XPS spectrum, AFM images and impedance data. The Supporting information is available free of charge.

AUTHOR INFORMATION

Notes

There are no conflicts to declare.

Corresponding Author

*Andriy Zakutayev. Email: Andriy.Zakutayev@nrel.gov. Materials Science Center, National Renewable Energy Laboratory, Golden, CO, 80401, USA

Author Contributions

The manuscript was written through contributions of all authors. All authors have given approval to the final version of the manuscript.

ACKNOWLEDGEMENTS

This work was authored by the National Renewable Energy Laboratory, operated by Alliance for Sustainable Energy, LLC, for the U.S. Department of Energy (DOE) under Contract No. DE-AC36-08GO28308. Funding provided by Funding provided by Vehicle Technologies Office, Hybrid Electric Systems Program. David Howell (Manager), Battery R&D, Brian Cunningham and Peter Faguy (Technology Managers), at the U.S. Department of Energy, Office of Energy Efficiency and Renewable Energy, are gratefully acknowledged. A portion of the research was performed using computational resources sponsored by the Department of Energy's Office of Energy Efficiency and Renewable Energy and located at the National Renewable Energy Laboratory. Computational resources of the National Energy Research Scientific Computing Center (NERSC), a U.S. Department of Energy Office of Science User Facility operated under Contract No. DE-AC02-05CH11231, are gratefully acknowledged. The views expressed in the article do not necessarily represent the views of the DOE or the U.S. Government.

REFERENCES

(1) Franco Gonzalez, A.; Yang, N.-H.; Liu, R.-S. Silicon Anode Design for Lithium-Ion Batteries: Progress and Perspectives. *The Journal of Physical Chemistry C* **2017,** *121*, 27775-27787, DOI: 10.1021/acs.jpcc.7b07793.
(2) Zhu, J.; Wang, T.; Fan, F.; Mei, L.; Lu, B. Atomic-Scale Control of Silicon Expansion Space as Ultrastable Battery Anodes. *ACS Nano* **2016,** *10*, 8243-8251, DOI: 10.1021/acsnano.6b04522.
(3) Cheng, X.-B.; Zhang, R.; Zhao, C.-Z.; Wei, F.; Zhang, J.-G.; Zhang, Q. A Review of Solid Electrolyte Interphases on Lithium Metal Anode. *Advanced Science* **2016,** *3*, 1500213-n/a, DOI: 10.1002/advs.201500213.
(4) Xu, W.; Wang, J.; Ding, F.; Chen, X.; Nasybulin, E.; Zhang, Y.; Zhang, J.-G. Lithium metal anodes for rechargeable batteries. *Energy & Environmental Science* **2014,** *7*, 513-537, DOI: 10.1039/C3EE40795K.

(5) Aurbach, D. Review of Selected Electrode–solution Interactions which Determine the Performance of Li and Li ion Batteries. *Journal of Power Sources* **2000,** *89*, 206-218, DOI: https://doi.org/10.1016/S0378-7753(00)00431-6.
(6) Xu, K. Electrolytes and Interphases in Li-Ion Batteries and Beyond. *Chemical Reviews* **2014,** *114*, 11503-11618, DOI: 10.1021/cr500003w.
(7) Yang, C. R.; Wang, Y. Y.; Wan, C. C. Composition Analysis of the Passive Film on the Carbon Electrode of a Lithium-ion Battery with an EC-based Electrolyte. *Journal of Power Sources* **1998,** *72*, 66-70, DOI: https://doi.org/10.1016/S0378-7753(97)02655-4.
(8) Young, B. T.; Heskett, D. R.; Nguyen, C. C.; Nie, M.; Woicik, J. C.; Lucht, B. L. Hard X-ray Photoelectron Spectroscopy (HAXPES) Investigation of the Silicon Solid Electrolyte Interphase (SEI) in Lithium-Ion Batteries. *ACS Applied Materials & Interfaces* **2015,** *7*, 20004-20011, DOI: 10.1021/acsami.5b04845.
(9) Lindgren, F.; Xu, C.; Niedzicki, L.; Marcinek, M.; Gustafsson, T.; Björefors, F.; Edström, K.; Younesi, R. SEI Formation and Interfacial Stability of a Si Electrode in a LiTDI-Salt Based Electrolyte with FEC and VC Additives for Li-Ion Batteries. *ACS Applied Materials & Interfaces* **2016,** *8*, 15758-15766, DOI: 10.1021/acsami.6b02650.
(10) Weadock, N.; Varongchayakul, N.; Wan, J.; Lee, S.; Seog, J.; Hu, L. Determination of mechanical properties of the SEI in sodium ion batteries via colloidal probe microscopy. *Nano Energy* **2013,** *2*, 713-719, DOI: https://doi.org/10.1016/j.nanoen.2013.08.005.
(11) Dupré, N.; Moreau, P.; De Vito, E.; Quazuguel, L.; Boniface, M.; Bordes, A.; Rudisch, C.; Bayle-Guillemaud, P.; Guyomard, D. Multiprobe Study of the Solid Electrolyte Interphase on Silicon-Based Electrodes in Full-Cell Configuration. *Chemistry of Materials* **2016,** *28*, 2557-2572, DOI: 10.1021/acs.chemmater.5b04461.
(12) Zhao, J.; Lee, H.-W.; Sun, J.; Yan, K.; Liu, Y.; Liu, W.; Lu, Z.; Lin, D.; Zhou, G.; Cui, Y. Metallurgically Lithiated SiO_x Anode with High Capacity and Ambient Air Compatibility. *Proceedings of the National Academy of Sciences* **2016,** *113*, 7408-7413, DOI: 10.1073/pnas.1603810113.
(13) Zhang, Y.; Li, Y.; Wang, Z.; Zhao, K. Lithiation of SiO2 in Li-Ion Batteries: In Situ Transmission Electron Microscopy Experiments and Theoretical Studies. *Nano Letters* **2014,** *14*, 7161-7170, DOI: 10.1021/nl503776u.
(14) Radvanyi, E.; De Vito, E.; Porcher, W.; Jouanneau Si Larbi, S. An XPS/AES Comparative Study of the Surface Behaviour of Nano-silicon Anodes for Li-ion Batteries. *Journal of Analytical Atomic Spectrometry* **2014,** *29*, 1120-1131, DOI: 10.1039/C3JA50362C.
(15) Philippe, B.; Dedryvère, R.; Gorgoi, M.; Rensmo, H.; Gonbeau, D.; Edström, K. Role of the LiPF6 Salt for the Long-Term Stability of Silicon Electrodes in Li-Ion Batteries – A Photoelectron Spectroscopy Study. *Chemistry of Materials* **2013,** *25*, 394-404, DOI: 10.1021/cm303399v.
(16) Delpuech, N.; Mazouzi, D.; Dupré, N.; Moreau, P.; Cerbelaud, M.; Bridel, J. S.; Badot, J. C.; De Vito, E.; Guyomard, D.; Lestriez, B.; Humbert, B. Critical Role of Silicon Nanoparticles Surface on Lithium Cell Electrochemical Performance Analyzed by FTIR, Raman, EELS, XPS, NMR, and BDS Spectroscopies. *The Journal of Physical Chemistry C* **2014,** *118*, 17318-17331, DOI: 10.1021/jp503949y.

(17) Seah, M. P.; Gilmore, I. S.; Beamson, G. XPS: Binding Energy Calibration of Electron Spectrometers 5—Re - evaluation of the Reference Energies. *Surface and Interface Analysis* **1998,** *26*, 642-649, DOI: 10.1002/(SICI)1096-9918(199808)26:9<642::AID-SIA408>3.0.CO;2-3.
(18) Schmid, M.; Steinrück, H. P.; Gottfried, J. M. A new asymmetric Pseudo - Voigt function for more efficient fitting of XPS lines. *Surface and Interface Analysis* **2014,** *46*, 505-511, DOI: 10.1002/sia.5521.
(19) Jain, A.; Ong, S. P.; Hautier, G.; Chen, W.; Richards, W. D.; Dacek, S.; Cholia, S.; Gunter, D.; Skinner, D.; Ceder, G.; Persson, K. A. Commentary: The Materials Project: A materials genome approach to accelerating materials innovation. *APL Materials* **2013,** *1*, 011002, DOI: 10.1063/1.4812323.
(20) Kresse, G.; Furthmüller, J. Efficient Iterative Schemes for Ab initio Total-energy Calculations Using a Plane-wave Basis Set. *Physical Review B* **1996,** *54*, 11169-11186, DOI: 10.1103/PhysRevB.54.11169.
(21) Blöchl, P. E. Projector Augmented-wave Method. *Physical Review B* **1994,** *50*, 17953-17979, DOI: 10.1103/PhysRevB.50.17953.
(22) Perdew, J. P.; Burke, K.; Ernzerhof, M. Generalized Gradient Approximation Made Simple. *Physical Review Letters* **1996,** *77* (18), 3865-3868, DOI: 10.1103/PhysRevLett.77.3865.
(23) Ong, S. P.; Wang, L.; Kang, B.; Ceder, G. Li−Fe−P−O2 Phase Diagram from First Principles Calculations. *Chemistry of Materials* **2008,** *20*, 1798-1807, DOI: 10.1021/cm702327g.
(24) Ong, S. P.; Richards, W. D.; Jain, A.; Hautier, G.; Kocher, M.; Cholia, S.; Gunter, D.; Chevrier, V. L.; Persson, K. A.; Ceder, G. Python Materials Genomics (pymatgen): A robust, open-source python library for materials analysis. *Computational Materials Science* **2013,** *68*, 314-319, DOI: https://doi.org/10.1016/j.commatsci.2012.10.028.
(25) Vinet, P.; Smith, J. R.; Ferrante, J.; Rose, J. H. Temperature Effects on the Universal Equation of State of Solids. *Physical Review B* **1987,** *35*, 1945-1953, DOI: 10.1103/PhysRevB.35.1945.
(26) Green, M. L.; Takeuchi, I.; Hattrick-Simpers, J. R. Applications of High-throughput (combinatorial) Methodologies to Electronic, Magnetic, Optical, and Energy-related Materials. *Journal of Applied Physics* **2013,** *113*, 231101, DOI: 10.1063/1.4803530.
(27) Green, M. L.; Choi, C. L.; Hattrick-Simpers, J. R.; Joshi, A. M.; Takeuchi, I.; Barron, S. C.; Campo, E.; Chiang, T.; Empedocles, S.; Gregoire, J. M.; Kusne, A. G.; Martin, J.; Mehta, A.; Persson, K.; Trautt, Z.; Van Duren, J.; Zakutayev, A. Fulfilling the Promise of the Materials Genome Initiative with High-throughput Experimental Methodologies. *Applied Physics Reviews* **2017,** *4*, 011105, DOI: 10.1063/1.4977487.
(28) Muster, T. H.; Trinchi, A.; Markley, T. A.; Lau, D.; Martin, P.; Bradbury, A.; Bendavid, A.; Dligatch, S. A Review of High-throughput and Combinatorial Electrochemistry. *Electrochimica Acta* **2011,** *56*, 9679-9699, DOI: https://doi.org/10.1016/j.electacta.2011.09.003.

(29) Carey, G. H.; Dahn, J. R. Combinatorial Synthesis of Mixed Transition Metal Oxides for Lithium-Ion Batteries. *ACS Combinatorial Science* **2011,** *13*, 186-189, DOI: 10.1021/co1000597.
(30) Martinez de la Hoz, J. M.; Leung, K.; Balbuena, P. B. Reduction Mechanisms of Ethylene Carbonate on Si Anodes of Lithium-Ion Batteries: Effects of Degree of Lithiation and Nature of Exposed Surface. *ACS Applied Materials & Interfaces* **2013,** *5*, 13457-13465, DOI: 10.1021/am404365r.
(31) Jaclyn Coyle, M. B., Christopher Apblett, Conrad Stoldt Investigating Chemical Reactivity of Lithium Silicate Model SEI Layers. **in preparation**.
(32) Yun Xu, K. W., Jaclyn Coyle, Chaiwat Engtrakul, Glenn Teeter, Conrad Stoldt, Anthony Burrell, Andriy Zakutayev. Early Stage Solid Electrolyte Interphase Formation on Lithium Lilicide. **in preparation**.
(33) Martinez de la Hoz, J. M.; Soto, F. A.; Balbuena, P. B. Effect of the Electrolyte Composition on SEI Reactions at Si Anodes of Li-Ion Batteries. *The Journal of Physical Chemistry C* **2015,** *119*, 7060-7068, DOI: 10.1021/acs.jpcc.5b01228.
(34) Sim, S.; Oh, P.; Park, S.; Cho, J. Critical Thickness of SiO2 Coating Layer on Core@Shell Bulk@Nanowire Si Anode Materials for Li-Ion Batteries. *Advanced Materials* **2013,** *25*, 4498-4503, DOI: 10.1002/adma.201301454.

Table of contents